Fuel 405 (2026) 136736

Contents lists available at ScienceDirect

Fuel

journal homepage: www.elsevier.com/locate/fuel

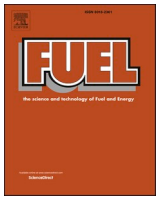

Full Length Article

Data-driven prediction of spray macroscopic characteristics for marine injectors using neural networks

Marilia G.J. Vaz [a,b,*], Ioannis Karathanassis [a,*], Manolis Gavaises [a], Gerard Mouokue [b]

[a] School of Science & Technology, City St' George's University of London, Northampton Square, London EC1V 0HB, United Kingdom
[b] Woodward L'Orange GmbH, Porschestraße, Stuttgart 70435, Germany

ARTICLE INFO

Keywords:
Machine-learning
Large diesel injectors
Spray penetration
Spray cone angle

ABSTRACT

Fuel flexibility ensures reliable operation and improves the implementation of a dual-fuel strategy alongside the Diesel-only model in marine powertrains. This versatile approach, however, imposes limitations related to the complexity of the injection system, underpinning the necessity of comprehending the relationship between design and performance to facilitate the injector optimization process. The present study introduces a data-driven predictor utilizing a deep neural network to predict spray tip penetration and cone angle in marine injectors. This neural network is trained using experimental data from serial and prototype industrial designs, incorporating operating conditions and a wide range of geometrical parameters as primary input features. Issues, as for example overfitting of the training dataset, were mitigated via regularization, enhancing generalization. The deep neural network accurately predicts spray characteristics across short, medium, and long penetration ranges, achieving 95% accuracy for unseen data. Furthermore, a feature importance analysis indicates that the injection pressure, number of spray holes, outlet spray hole diameter, and sac hole volume are the primary parameters influencing spray behavior. This neural network provides a computationally efficient alternative to conventional approaches, such as time-consuming Computational Fluid Dynamics simulations or test measurements. The model is tailored to support the marine injector design workflow, allowing the fast exploration of design space in the early design phase at operation conditions relevant for fuel flexibility, and contributing to accelerate the injector development process.

1. Introduction

The diesel engine has been established as the predominant power source in the marine sector, mostly due to its reduced risk of fire hazard and its capacity to operate with a variety of fuels [1]. Fuel flexibility offers operational versatility and economic advantages, enabling the engine to operate with Heavy Fuel Oil (HFO), Marine Fuel Oil, Intermediate Fuel Oil, Marine Diesel Oil, and Marine Gas Oil [2].

Nonetheless, the petroleum-derived fuels currently employed in the marine sector substantially contribute to global emissions [3]. They raise concern about air quality and human health, particularly because the release of deleterious particulate matter, alongside the production of nitrogen oxides and sulfur oxides [4]. In order to address these issues, it is essential to reevaluate the fuel selection for marine engines and the fuel injection system as a whole, since it directly influences both performance and emissions [5,6]. Biodiesel serves as an alternative fuel to reduce emissions owing to its renewable nature and cleaner combustion properties. Nevertheless, the maritime sector must overcome significant obstacles associated with the extensive use of biodiesel, mostly concerning cost, feedstock sustainability, increased Nitric oxides (NOx) emissions and lower engine efficiency [7,8]. Dual-Fuel Internal Combustion Engines (DFICE) offer a viable solution for the marine sector, facilitating advancement towards a more sustainable and environmentally friendly future while maintaining operational efficiency.

The DFICE configuration relies on a primary fuel with high octane number to supply the majority of energy and designate the combustion conditions. The pilot fuel, commonly a minimal amount of Diesel, serves as an ignition source [9]. The DFICE concept enables seamless transitions between traditional fuels such as HFO and more eco- friendly alternatives like liquefied natural gas, hydrogen, or biofuels during engine operation [10]. This versatility allows the selection of the most cost-effective fuel option based on its availability, price fluctuations, and regulatory considerations [11].

However, the fuel flexibility embedded in the DFICE concept entails disadvantages related to the complexity of the injection system. Diesel

* Corresponding authors.
E-mail addresses: Marilia.Justino-Vaz@citystgeorges.ac.uk (M.G.J. Vaz), Ioannis.Karathanassis@citystgeorges.ac.uk (I. Karathanassis).

https://doi.org/10.1016/j.fuel.2025.136736
Received 21 April 2025; Received in revised form 22 August 2025; Accepted 2 September 2025
Available online 11 September 2025

Nomenclature

ANN	Artificial Neural Network
CFD	Computational Fluid Dynamics
CVC	Constant Volume Chamber
DNN	Deep Neural Network
DBI	Diffuse-Backlight Illumination
DFICE	Dual-Fuel Internal Combustion Engines
HFO	Heavy Fuel Oil
ML	Machine Learning
MAPE	Mean Absolute Percentage Error
NOx	Nitric Oxides
ReLU	Rectified Linear Unit
SCA	Spray Cone Angle
STP	Spray Tip Penetration

direct-injection concepts can be materialized by either utilizing two fuel injectors, with one of them placed in a decentralized location inside the combustion chamber, or by employing a single injector with an intricate internal flow path including a series of nozzles and potentially more than one needles. The increase in complexity for the fuel injector hardware, cost and reduced performance for a not symmetric combustion process, hinders the wide adoption of the latter strategy. Utilizing a single injector equipped with a single nozzle and needle for both Diesel-only and pilot DFICE operation presents the best trade-off between system simplicity and performance. While a single injector simplifies system design, reduces weight and volume, and potentially lowers costs. It also introduces challenges associated with the accurate metering of both large and small fuel quantities, the increased risk of nozzle clogging and the inevitable compromise in spray atomization, particularly at low flow rates.

Understanding the relationship between nozzle geometry, flow dynamics, fuel delivery and spray characteristics provides additional critical insight on injector optimization and is a necessary step towards optimizing the spray trade-off characteristics for fuel flexible operation. Spray tip penetration is a critical element in the fuel injection process, as it directly influences air–fuel mixing, combustion efficiency, and, consequently, engine performance and emissions [12,13]. Over the past few decades, researchers have been dedicated to developing mathematical models to predict spray tip penetration and spray cone angle. Such efforts have been intensified in recent years owing to the increasing sophistication of computational tools and the introduction machine learning techniques.

The traditional methods for predicting Spray Tip Penetration (STP) and Spray Cone Angle (SCA) often rely on empirical correlations, semi-empirical models, and high- fidelity Computational Fluid Dynamics (CFD) simulations. Empirical correlations are frequently derived from experimental data and adjusted to fit certain operating ranges. They are user-friendly and computationally inexpensive. However, their accuracy is limited when applied to conditions that diverge from those employed for their derivation. Semi-empirical models, such as those derived by Wakuri et al. [14] and Hiroyasu et al. [15], combine simplified physics with empirical correlations. The incorporation of considerations such as momentum theory and jet disintegration theory enable these models to reflect more aspects of the underlying physics, going beyond empirical correlations. Nonetheless, they remain dependent on some empirical attributes and may lack precision in highly varying injection conditions [16].

CFD can be leveraged to model interactions between the liquid fuel jet, surrounding gas, and turbulence, providing comprehensive insights into spray breakup, atomization, and droplet dynamics [17]. This detailed approach supports the prediction of spray characteristics across diverse operating conditions and injector designs, surpassing the constraints of empirical correlations. However, numerical simulations can be computationally demanding and time- consuming, particularly for high-fidelity approaches [18]. Their precision is significantly influenced by the selected turbulence and break-up sub-models and necessitate validation against experimental data to ensure their reliability [19].

Data-driven modeling techniques, in particular Machine Learning (ML), have demonstrated significant potential in accurately predicting the STP and SCA, while effectively capturing intricate interactions among input parameters such as injection pressure, nozzle shape, and fuel characteristics. It serves as an attractive alternative for performing the injection equipment design and optimization, in contrast to costly and time-intensive experimental measurements and CFD simulations [20].

Along these lines, Nowruzi et al. [21] have investigated different architectures of Artificial Neural Network (ANN) to estimate the average STP and SCA of a single nozzle injector. The input parameters for training the supervised feed-forward network using the back-propagation method included nozzle diameter, injection pressure, injection profile, back pressure, and ambient temperature. Hwang et al. [22] employed a regression model to predict the liquid penetration length, liquid width, and three-dimensional distribution of spray liquid fraction of a multi-hole gasoline injector. Their model included nine input features (fuel properties such as density and viscosity, along with ambient variables), showing remarkable concordance with experimental data.

Lie et al. [23] derived a mathematical equation for STP via a back-propagation neural network for biodiesel and diesel mixtures. They modeled a single-hole injector, where the input parameters were the fuel characteristics and injection pressure. This model was sub-sequently enhanced by Richards and Emekwuru [24] due to the limited experimental training data. They mitigated overfitting problems from the prior model with a systematic approach to uncertainty.

Khan et al. [25] evaluated the efficiency of four machine learning methods (random forest, extreme gradient boosting, multilayer perceptron, and elastic net) in predicting STP and SCA. Although their study focused on single and dual hole injectors, they utilized only two geometric characteristics as inputs: normalized nozzle outlet diameter and conicity. Hence, simplifying those injectors to single hole configurations in their models. Zhang et al. [26] examined the sensitivity of parameters in a genetic algorithm backpropagation neural network for predicting spray penetration, comparing its performance with semi-empirical methods. Their model utilized experimental data from a single hole injector, with the ANN model incorporating operational variables and fuel properties as input parameters.

Tian et al. [27] conducted an experimental research of octanol-diesel mixture, resulting in five fuel compositions. Those fuels were tested in different operation conditions for a single hole injector. Then, this data was used to train an ANN and used it to compare the influence of octanol ratio on the spray characteristics. Zhang et al. [28] employed an ANN to predict the spray characteristics and vaporization index. The model was trained with data of five alcohol fuel and gasoline blends across a range of operation conditions for one multi-hole injector design, focusing on the physicochemical fuel properties as the main input features. Later, Zhang et al. [29] compared the response surface methodology with an ANN to predict the spray performance for the same fuels, where both models presented a high accuracy. Leng et al. [30] compared the experimental data of STP for a methanol injection at different operation conditions with Wakuri et al. [14] and Hiroyasu and Arrai [15] semi-empirical formulation. Due to the low precision of those formulations for methanol, a variation of convolutional neural network was proposed, reaching a better correlation with the experimental measurements.

Albeit the previous investigations, the semi-empirical models as well as the ML restrict themselves to few designs during their formulation, most of them to one or two injector designs. In addition, those models present a limited number of nozzle geometrical parameters as inputs.

They focus more on the impact of different operation conditions or fuels type. Varying designs is inherently a more complex task than adapting to different operational conditions for a single, fixed geometry because of the dimensionality increment [31,32]. Each design leads to more complex feature interactions and non-linear relationships, presenting a more challenging task. Therefore, their use is very restricted during the pre-development phase of injector designs, making it difficult to take advantage of the fast prediction to explore design range and identify the promising designs effectively during the optimization process.

Even though ML offers superior flexibility for spray macroscopic predictions compared to semi-empirical models, the elevate number of input parameters imposes an additional complexity. The collinearity among geometric parameters may destabilize the model, and this can normally be compensated by increasing the data set size [26]. On the other hand, high-quality data acquisition can be expensive and time-consuming, introducing limitations to the data expansion [25,33]. Setting up experiments or running simulations often requires significant resources. Another option is the usage of historical data or integrating it from different sources, but this task can be demanding due to differences in data formats and structural inconsistencies [34]. Hence, balancing the ML model complexity and generalization ability becomes a critical challenge.

Moreover, models in the literature are more commonly developed for light-duty applications due to their dominance in the market. Heavy-duty and marine injectors often operate over a much wider range of conditions than light-duty injectors, including variable fuel amounts, high injection pressures, and more severe environments [35]. Consequently, the accuracy of the those models are reduced for this specific type of injectors, making their extrapolation or tuning a time-consuming process without guaranteeing accurate results.

Therefore, the aim of this study is to develop a tool tailored for marine diesel injectors, which permits reliable predictions of spray macroscopic characteristics (STP and SCA) as well as a relative comparison of different designs under operating conditions relevant for fuel flexibility: Diesel-only and DFICE mode. The injector type explored in this study is typically used for small to medium sized four-stroke marine engines, with an average displacement volume of 5L per cylinder. To this goal, a deep neural network has been conceited and trained with experimental data from a variety of marine injector designs and operation conditions. The high-quality data, selection and feature engineering are the primary factors influencing the model performance, and in complement to the neural architecture, allowed the inclusion of 14 input features. Finally, focusing on the model applicability during the pre-development design phase, 10 of the input features are related to geometrical constrains to the conceptualization phase. This unique characteristic allows the usage of the model to on-the-fly explore the design range for marine injectors, which offers an advantage over the current semi-empirical models or neural networks in the literature.

2. Brief overview on spray tip penetration models

Wakuri et al. [14] and Dent [36] were among the first to establish semi-empirical models utilizing experimental data to establish a foundational knowledge of STP. Wakuri et al. [14] derived a STP correlation utilizing moment theory. Their formulation defined penetration as a function of the spray angle and the square root of the product of the spray hole diameter and time. Dent [36] maintained square root dependence and incorporated the effects of both evaporating and non-evaporating conditions in his formulation by considering the ambient temperature.

Hiroyasu and Arrai [15] presented a more advanced methodology by categorizing the formulation of STP into two separate regions: pre-break-up and post-break-up. Their formulation was based on experimental data and Levich's jet disintegration theory, and continues to serve as a foundation for numerous enhanced models. Naber and Siebers.

[37] significant modified the Wakury et al. [14] formulation together with Hiroyasu and Arrai [15]. They established a correlation for non-vaporizing STP based on a theoretical model derived from penetration time and length scales. Their correlation considers factors like ambient gas density and injection pressure. A significant contribution of their study is the inclusion of a term related to the injector opening time, which influences the initial penetration and enhances predictions in the the near-nozzle region.

Similary to Hiroyasu and Arrai, Desantes [38] categorized the diesel STP into two distinct regions, presenting a formulation based on basic fluid dynamic principles and dimensional analysis. Their model accounts for the impact of variables such as ambient gas density, injection pressure, and nozzle equivalent diameter on STP, while also considering the spray cone angle and its effect on penetration length.

For large marine-type injectors, Najar at al. [39] propose a model correlating the STP as a function of the cumulative injected mass, providing an alternative viewpoint to conventional time-dominated studies. Zhang et al. [40] also provided a formulation specifically tailored for large-sized injectors. They developed updated correlations for the model proposed by Hiroyasu and Arrai [15]. These correlations take into account variables such as ambient gas density and temperature, which are essential for marine engine applications.

In summary, typical parameters among these formulations often incorporate injection pressure (or a related metric such as momentum flux), nozzle orifice diameter, and ambient gas density. However, they remain limited in applying more geometrical factors to their formulation. These shared parameters reflect the fundamental physical factors influencing spray development, such as the initial momentum of the fuel jet, the resistance imposed by the surrounding gas, and the duration of injection.

3. Brief overview on spray angle models

Similar to the STP, early models for spray angle often relied on simplifying assumptions, treating the spray as a solid cone with a constant angle. As experimental data became more accessible, researchers began to integrate empirical correlations. Wakuri et al. [14] incorporated elements of both empirical correlations and moment theory in their formulation, where the ambient gas density has a significant impact on the spray cone angle.

Varde et al. [41] have enhanced the comprehension of spray behavior, specifically on the impact of nozzle geometry using the spray hole length and diameter ratio L/D. These investigations frequently study the correlation among spray angle, injection pressure, orifice dimensions, and the characteristics of both the liquid and the surrounding gas. The formulation of Hiroyasu and Arai [15] is a part of a more comprehensive model that also incorporates STP. However, they proposed a simplified model that assumes a constant spray cone angle prior to the primary breakup of the spray. Naber and Siebers [37] provide insights into the relationship between the spray cone angle and other spray characteristics. Although they do not offer a specific formula for the cone angle, their research establishes a framework for comprehending its correlation with STP and dispersion, especially in connection to gas density and vaporization effects. According to Arrègle et al. [42], the spray cone angle is affected primarily by injection pressure, ambient gas density, spray hole geometry (length and diameter), and needle lift. Unlike earlier investigations, they found that the spray hole diameter had a significant effect. Due to constant wall thickness in their studies, spray hole length-to-diameter ratio is a significant geometric parameter.

Overall, parameters which are commonly evaluated in these formulations typically include injection pressure, spray hole geometry (diameter and length or related ratios), and the density ratio between the fuel and the surrounding gas. Moreover, backpressure is a critical factor in these formulations, as it influences the penetration and dispersion of the spray. Nevertheless, the specific dependencies and exponents in these correlations may vary, reflecting differences in

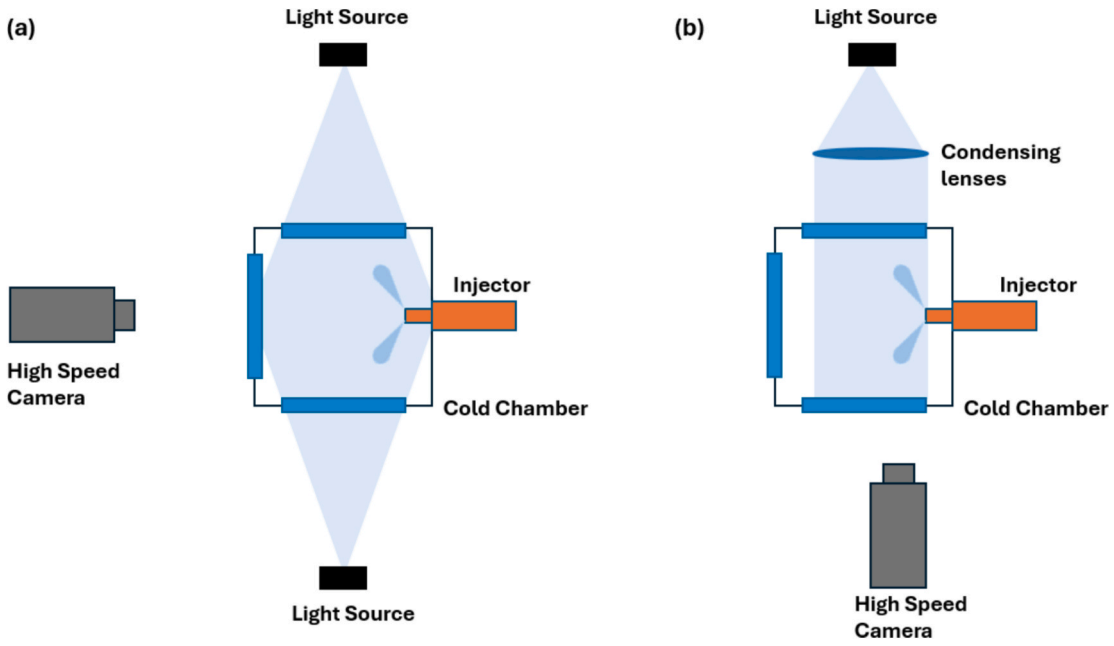

Fig. 1. Schematic layout for the optical measurements at Woodward L'Orange: (a) Mie-scattering Light, (b) DBI. (For interpretation of the references to colour in this figure legend, the reader is referred to the web version of this article.)

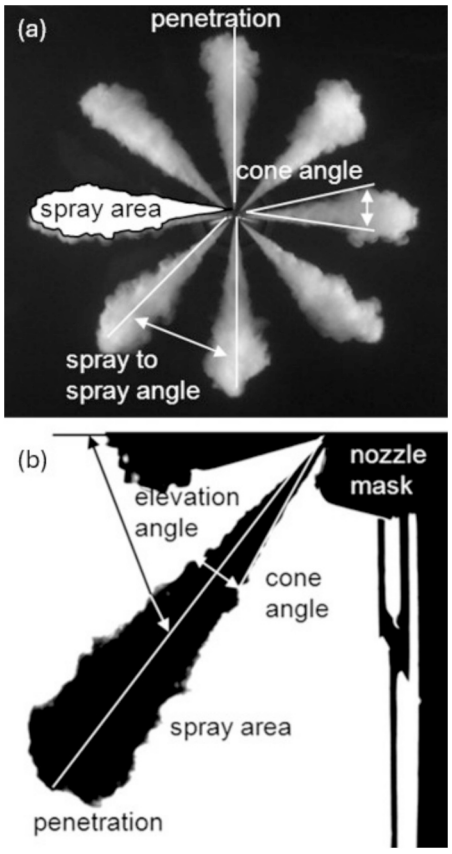

Fig. 2. Indicative images: (a) Mie-scattering, (b) DBI.

experimental setups, measurement techniques, and the conditions investigated.

4. Experimental data acquisition

This study used the past decade of experimental testing, encompassing serial and prototype designs from Woodward L'Orange, to train the neural network. The resulting data acquired using optical methods is described in subsections 4.1 to 4.3, which offer a concise summary of the optical setup, image processing, and operational conditions for liquid-to-gas measurements.

4.1. Experimental configuration

The spray-propagation optical measurements were performed in a sealed cubic Constant Volume Chamber (CVC) with a total capacity of 34 L. This CVC comprises three optical windows made of fused silica panes, each measuring 200 mm by 200 mm. The temperature and pressure were controlled via a valve-regulated nitrogen supply and cooling- water circulation, respectively. The chamber, designed to withstand pressures up to 60 bar, enabled optical diagnostics of spray behavior under controlled conditions, encompassing representative values of in-cylinder pressure during diesel injection. The chamber temperature was maintained constant at 293.15 K.

Fig. 1 depicts the schematic of the optical configuration employed for the visualization and quantification of the spray using Mie-scattering (Fig. 1a) and Diffuse-Backlight Illumination (DBI) (Fig. 1b). The camera, is positioned perpendicular to the light path and opposite to the injector for the Mie-scattering approach. In DBI, a collimated light beam illuminated the spray, and the resultant back-projection were recorded by the high-speed camera. The camera employed is a Photron FASTCAM SA5, capable of operating at frequencies up to 775,000 fps, while the injection process is controlled by a custom-engineered ECU system. The synchronization between the injection system and the camera guaranteed precise temporal resolution of the spray development, utilizing the injector trigger signal as a reference for capturing the image sequences.

This adaptable optical configuration facilitated thorough viewing and quantification of spray dynamics, yielding essential data for the validation of computational models and the optimization of injector

Table 1
Fluid properties of the SRS Calibration Fluid CV in comparison to Diesel ([a]value at 15 °C; [b]value at 40 °C) [46,47].

Fuel Properties	SRS	Diesel
Density [kg/m^3]	824[a]	820 – 850[a]
Viscosity [mm^2/s]	2.52[b]	1.9 – 4.1[b]

Table 2
Operating conditions explored in the spray optical measurements.

Parameter	Min.	Max.
Electrical pulse duration [μs]	220	1200
Injection Pressure [bar]	800	2200
Ambient Pressure [bar]	25	60
Temperature [K]	Constant at 293.15	
Repetitions [-]	5	10
Injector type [-]	27 multi-holes injectors from serial and prototype industrial designs	

designs for marine diesel engine applications. The combination of DBI and Mie-scattering enables the visualization of both macroscopic spray attributes and microscopic droplet characteristics.

4.2. Image processing method

An in-house software was developed to monitor the spray boundary across numerous frames, offering temporal data regarding the spray evolution. Following image processing, quantifiable data were extracted from the temporal variation of the spray. In general, the image processing is composed of three main stages: acquisition of the background image for comparison of the gray value of the pixels of each image, definition of the spray contour based on a threshold intensity-sensitive method [43] and calculation of the macroscopic variable. The two last stages are repeated for each time-step until the end of injection.

Fig. 2a illustrates an indicative processed image obtained by Mie-scattering. The intensity of the dispersed light correlates with the concentration of droplets. The threshold was selected on the pixel intensity difference based on the background value and empirically determined to differentiate between spray and gas areas. Based on this pixel comparison, the spray border is delineated according to the intensity of dispersed light. This technique enables the viewing and quantification of liquid phase penetration, particularly in dense sprays where DBI may be constrained by the spray's opacity.

In a similar manner, DBI is normally utilized to determine the area of the spray with adequate droplet concentration to be classified as part of the spray plume. Fig. 2b illustrates an indicative processed image obtained by DBI. The spray image appears as a darker area contrasted against a lighter background. Image processing is utilized to augment contrast and delineate the spray boundary. Again, the threshold was selected based on the background value and empirically depicted to differentiate between the spray and gas areas. However, DBI cannot discriminate between the liquid core of the spray and the evaporating surrounding area.

These optical techniques are employed to determine STP, SCA, spray area, spray circumference, spray-to-spray deviation, and shot-to-shot deviation. The STP was defined as the furthest pixel from the spray hole exit. In this work, SCA was measured at the intersection of the spray axis and the center of mass based on the 2D representation image of the spray area. This strategy reduces the dependence on arbitrary thresholding or images segmentation choice [44]. Finally, the macroscopic spray variables of the multi-holes injectors are the average of each spray holes in the case of Mie-scattering measurement.

4.3. Operation conditions

The CVC facilitates the evaluation of diverse marine injectors, enabling a comparison of their spray characteristics and potential impact on combustion performance. For all cases, diesel fuel was substituted with a SRS Calibration Fluid CV during the optical measurements. This fluid presents a very close viscosity tolerance and meets the ISO standard 4113-CV-AW. Calibration fluids are typically formulated to be less opaque than diesel, facilitating clearer viewing of the spray structure by optical techniques. Furthermore, they have well-defined and consistent physical properties, as shown in Table 1. In addition, Calibration Fluids exhibit lower flammability and toxicity compared to diesel, and are more economical than specialized research-grade diesel fuels [45]. This substitution is essential to ensure consistence, reliability and results standardization of the testing.

In those measurements, the electronically triggered injectors exhibited an electrical pulse duration, excluding latency time, ranging from 220 μs to 1200 μs. A range of injection pressures, from 800 to 2200 bar, was investigated to distinguish the spray behavior throughout different operating regimes. The ambient pressure within the chamber was also altered. The temperature remained constant at 293.15 K due to the properties of this CVC, also referred to as a cold chamber, while the density was regulated by adjusting the pressure between 25 and 60 bar to simulate realistic engine conditions. Prior to each experiment, the chamber was purged and filled with nitrogen to a specified pressure and temperature, guaranteeing a uniform and inert atmosphere. Finally, each measurement was repeated between 5 and 10 times for each working condition to ensure reliability. Table 2 summarizes the injection conditions utilized in all experimental measurements.

5. Exploratory data analysis

In this study, the integration of historical data from numerous sources proved to be a time-consume task. The partnership with Woodward L'Orange allowed the access to a comprehensive and detailed geometric description in parallel to the design process. The experimental data from multiple projects were cross-referenced with the database of the design department. During data standardization, the main issues encountered were insufficient data descriptions, improper formatting, duplicate entries, and outdated documentation. Consequently, the relevance of the datasets was considered in the data analysis.

Currently, data preparation problems are crucial in ML applications. Data collection and cleaning constitute near 80–90 % of the total effort [34]. Once the data were curated, ensuring suitable format, size, and quality, 85 experimental measurements were selected, with each measurement varying between 11 and 90 data points based on the injection duration. Those measurements covered a total of 27 distinct injector designs, which include serial and prototypes designs. The input features were selected based on feature reduction, profiling (assumptions derived from in-house expertise), and the importance of the variables for this study.

The final dataset had 14 input elements, including three operational conditions, ten design parameters, and the time after energization. The operational parameters are electrical pulse duration, injector rail pressure, and ambient pressure as

already shown in Table 2 and delineates the injection conditions utilized during the experimental measures. The design parameters include sac hole volume, k-factor, number of spray holes, angle between spray holes, Q100, throttle effect, inlet spray hole diameter, output spray hole diameter, sac hole area, and minimum distance between spray holes. For reasons of confidentiality, the specific range of design parameters must be undisclosed because of cooperation with an industrial partner.

In addition, three of those features are the result of transforming data into relevant information and the minimum requirements in the early

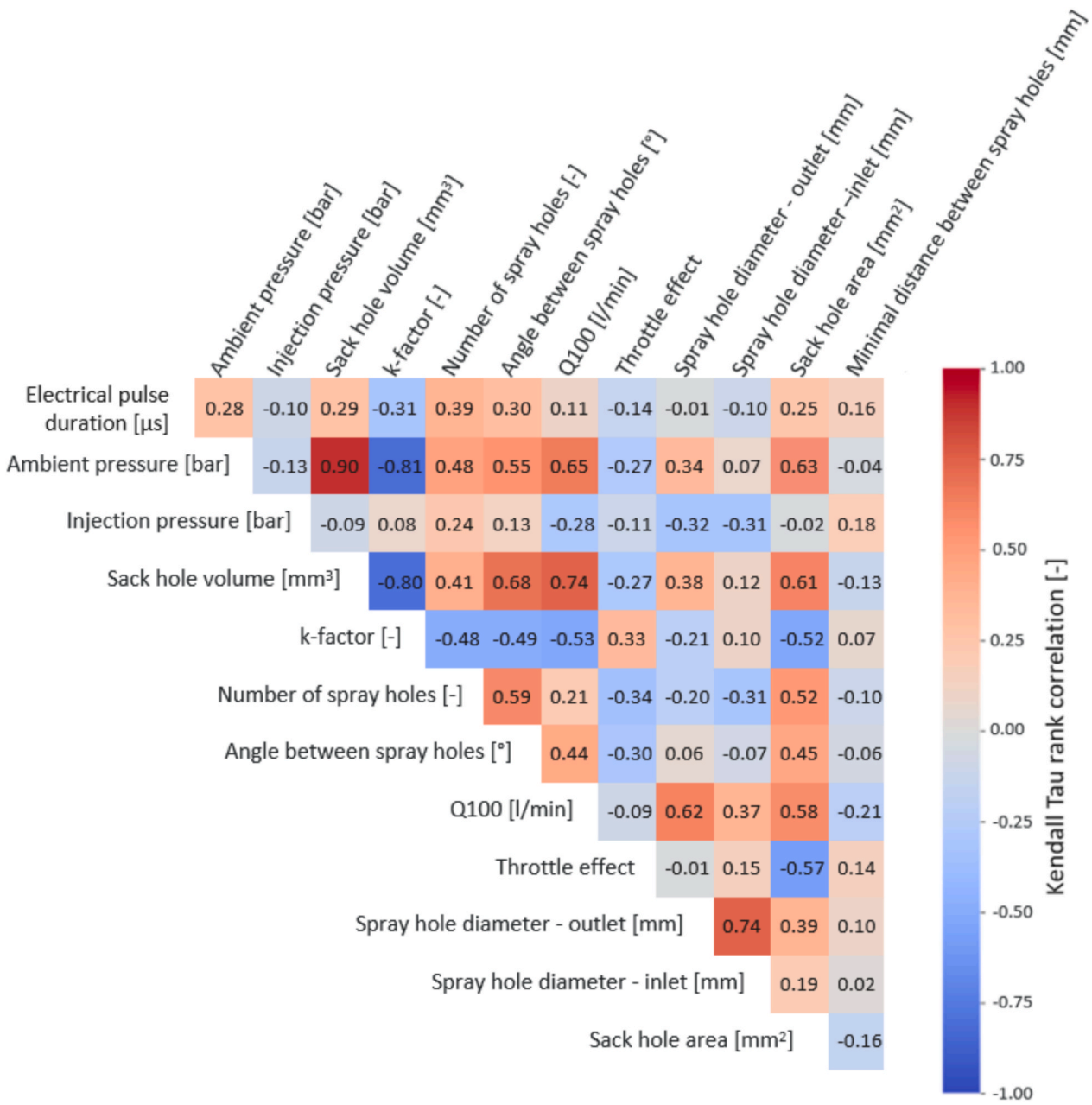

Fig. 3. Kendall Tau's rank correlation coefficient for the selected features. operating conditions and geometrical parameters.

phase of the design process. The k-factor, (also referred to as conicity), denotes the hole taper degree and can be expressed as:

$$K_{factor} = \left(\frac{D_{in} - D_{out}}{L}\right) x100 \tag{1}$$

where L denotes the length of the spray hole, D_{in} and D_{out} represent the inlet and outlet diameters of the spray hole, respectively. The Q100 is the expected mass flow rate of the injector measured at a pressure differential of 100 bar. This number serves as a reference point throughout the injector design conceptual phase and offers a standardized assessment of diesel injector performance.

The throttle effect is the third one and is also a projected performance established at the conceptual phase. This dimensionless quantity is derived from the theoretical velocity according to Bernoulli's Equation and the anticipated mass flow rate:

$$Throttle_{effect} = \frac{\frac{Q_{100}}{n_{holes}}}{A_o} \cdot \sqrt{\frac{\rho}{2\Delta P}} \tag{2}$$

where n_{Holes} is the number of spray holes, A_{o} represents the area of the spray hole, ρ signifies the fluid density, and ΔP indicates the pressure differential, which in this preliminary phase is 100 bar.

The redundancy among selected input features can be assessed by statistical correlation. Feature correlation is essential for the efficacy and interpretability of machine learning models. A reduced correlation among input characteristics could simplify the system equations in training algorithms, potentially facilitating resolution, enhancing convergence rates, and improving generalization [48]. Fig. 3 illustrates the Kendall tau's rank correlation among the operation conditions and geometrical input features. Kendall rank correlation is a non-parametric test that assesses whether a monotonic relationship exists between two variables or not [49]. Kendall tau is a suitable option for correlation

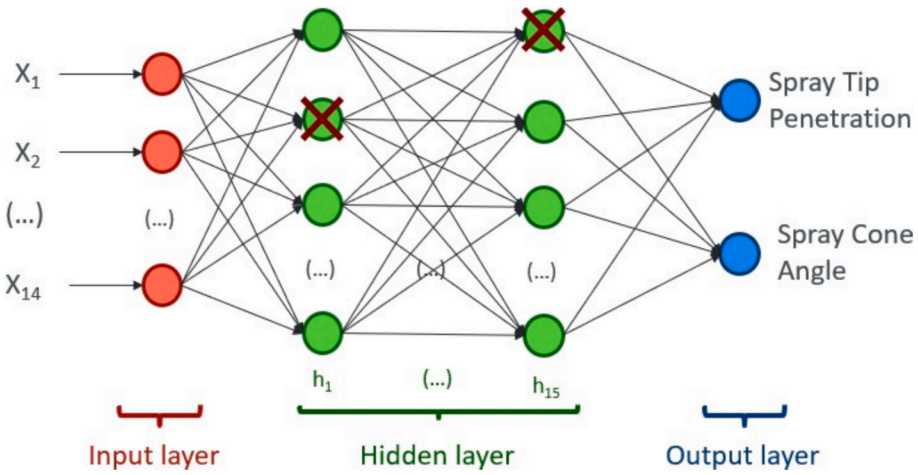

Fig. 4. Representation of the neural network consisting of one input layer, ten hidden layers and one output layer, with dropout nodes symbolized by red marks. (For interpretation of the references to colour in this figure legend, the reader is referred to the web version of this article.)

analysis in small datasets, in contrast to other formulations such as Spearman's correlation coefficient (rho) [50]. This method does not presuppose a linear relationship or normal distribution, providing narrower confidence intervals, better control over Type I errors, and robustness to outliers [49,51]. Kendall tau's rank correlation can be mathematically defined as:

$$\tau = \frac{n_c - n_d}{n(n-1)/2} \tag{3}$$

where n_c reflects the number of concordant pairs, n_d represents the number of discordant pairs, and n signifies the sample size. This formulation results in a value such that $-1 \leq \tau \leq 1$. A coefficient of ± 1 signified a strong monotonic relationship. Conversely, an opposite directional growth signifies a perfect negative correlation, while 0 indicates the absence of a monotonic relationship between the variables. It has to be underlined that the specific metric detects patterns between the input data, without necessarily implying that such correlations are always representative of physical processes. They could also be indicative of intrinsic biases present in the experiment conducted to formulate the training data set.

As illustrated in Fig. 3, the majority of the characteristics exhibit weak to moderate correlations, with scores below $\pm$ 0.65. Among the operational conditions, only the ambient pressure exhibits strong correlations with certain design parameters, particularly with sac hole volume (0.90) and k-factor (-0.81). Nevertheless, this elevated correlation coefficient could be misled due to the diminished variability of those features.

Regarding the design parameters, the k-factor also exhibits a high correlation with sac hole volume (-0.80). The sac hole volume also shows a high correlation with the angle between the spray holes (0.68) and Q100 (0.74). The correlation between the inlet spray hole diameter and the outlet spray hole diameter reaches a value of 0.74, which aligns with the expectations, as they are interconnected through the K-factor specification.

Features that are highly correlated might diminish model interpretability, elevate the danger of overfitting, and induce multicollinearity, complicating the assessment of each feature's individual impact on the target variable [52,53]. Nonetheless, maintaining them can be advantageous, particularly in scenarios where feature interactions are complex, since eliminating correlated features may result in the loss of critical information [54]. Furthermore, their utilization is justified in contexts where they convey critical information and offer substantial insights into the model's interpretation and prediction [55]. Consequently, although certain features exhibited heightened correlation, the choice was made to preserve them owing to their importance in the design process.

6. Deep neural network architecture

Inspired by the brain synapses, ANN and Deep Neural Network (DNN) are subsets of ML, which consist of interconnected groups of artificial neurons. Both methods are capable of identifying patterns, categorizing data, and forecasting outcomes based on existing data [56]. DNNs are distinguished by their deep architecture, which allows them to handle more complex data and tasks [57]. In this work a multilayer perception or fully connected, feedforward neural network was employed. The topological configuration of the DNN consists of an arrangement of neurons in a network of hierarchical layers (input, hidden and output layers) with a 14-x-2 architecture, where x represents the variable number of neurons in the hidden layer, while 14 and 2 correspond to the neurons of the input and output layers. The 14 input parameters that constitute the input layer were described in the preceding section. The objective of this DNN is to be a preliminary tool for the injector design process, correlating the geometrical parameters and operational conditions to STP and SCA. Consequently, the output layer comprises the intended predictions, i.e., STP and SCA.

In the development of the DNN architecture, the number of neurons and hidden layer were adjusted, with 15 hidden layers providing the optimal balance of accuracy as presented in Appendix A. A low number can lead to underfitting, wherein the network does not adequately discern the underlying patterns within the data [58]. Increasing the number of hidden layers can enhance the network's capacity to model complex functions, however only to a certain extent. An excessive quantity of layers may lead to overfitting, where the network assimilates the noise present in the training data instead of the actual signal. Computational cost may increases excessively without considerable enhancement in accuracy [59].

Fig. 4 shows the schematic structure of the DNN, where based on their connection, the outputs from the previous layer serve as composite features for each neuron in the subsequent layer.

The LeakyReLU activation function, a variation of the Rectified Linear Unit (ReLU), was utilized in every neuron within a layer to introduce non-linearity, enabling the network to learn complex patterns. This function is available in the Keras library and aids in mitigating problems associated with inactive neurons. Neurons may occasionally become inactive during training; permitting a minimal non-zero gradient for negative inputs alleviates the issue of "dying ReLUs" [60].

Furthermore, two regularization techniques were employed to mitigate overfitting issues arising from the limited data available. The dropout rate was the first regularization technique employed, wherein

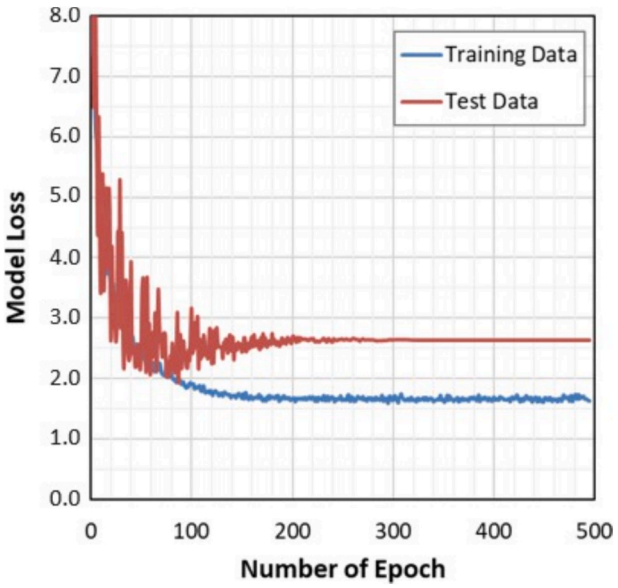

Fig. 5. Training and test-data loss curve of the DNN as a function of the number of Epochs.

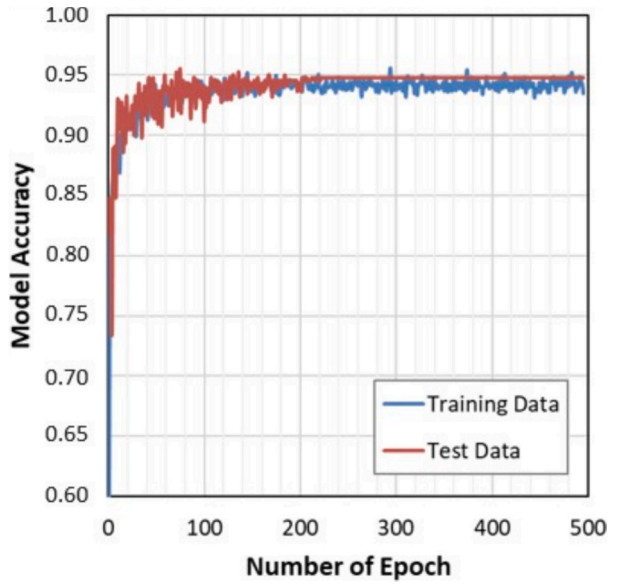

Fig. 6. Training and test-data accuracy curve of DNN as a function of the number of Epochs.

nodes randomly cease to transmit their forward signal during training with a 30 % probability, refer indicatively to the nodes annotated in the schematic DNN representation of Fig. 4. Consequently, following each update during training, the layers are arranged in a marginally altered configuration, allowing network layers to co-adapt in order to rectify errors from the preceding layer [61]. This hyperparameter mitigates excessive co-adaptation of units by randomly deactivating them, hence reducing overfitting and enhancing generalization on novel data [62].

The second regularization technique employed was early stopping. This cross-validation strategy terminates training when the model's performance no longer enhances over multiple consecutive epochs. Traditionally, this involves using a validation set to monitor performance. Nonetheless, the exclusion of a validation set, as implemented in this study, decreases computing time, which is beneficial in scenarios with limited data or noisy labels [63].

In the DNN training, the 85 experimental cases were randomly split into two datasets: 80 % for training and 20 % for testing. The data division was executed with careful precision to guarantee that all penetration ranges (short, medium, and long) were represented in both data sets. The test set was entirely unexposed during the training phase, enabling an objective evaluation of network performance. Additionally, prior to training the DNN model, the input data were standardized to the range [0,1], providing a uniform scale and appropriately representing the significance of each variable. This range aligns with the parameters of the employed activation function. The standardization was done by min–max normalization as given as:

$$x' = \frac{x - min(x)}{max(x) - min(x)} \tag{4}$$

where x is the original value, x' is the normalized value. This is especially significant in training deep learning models, because steady gradient computations are essential for effective learning, mitigating problems such as vanishing and exploding gradients [64].

The model loss was calculated via Mean Absolute Percentage Error (MAPE). This metric measures the average magnitude of errors between predicted and actual values, expressed as a percentage. The MAPE can be defined as follows:

$$MAPE = \frac{1}{n}\sum_{i=1}^{n}\frac{|y_i - Y_i|}{|y_i|}.100\% \tag{5}$$

where n denotes the number of data points in the training dataset, y_i represents the predicted output value of the DNN model, and Y_i the target value. A value near 0 denotes negligible error. The percentage error will significantly increase in the presence of outliers, as it is particularly sensitive to anomalous results.

7. Results

7.1. DNN evaluation

A comprehensive view of the training progress and performance of the neural network is illustrated in Fig. 5 and Fig. 6. The loss function quantifies the difference between the predicted output of the neural network and the actual, physics-derived, target values using MAPE. The downward trend seen with increasing number of epochs, as depicted in Fig. 5, indicates effective error minimization between predictions and actual values for the training data, obtaining a MAPE of 1.67. The respective value for the test data is 2.63. Approximately 300 epochs into training, the model attains a plateau in its predictions, indicating that additional training does not substantially enhance its performance. The model executes 200 additional epochs owing to the patience definition, a hyperparameter employed in the early stopping technique.

Early stopping terminates the training process when the loss no longer improves, while the patience value specifies the number of extra epochs to continue training following the last improvement in model loss [65]. Increased patience settings afford the model additional time to potentially enhance performance. In contrast, diminished patience values may cause premature stopping, leading to suboptimal model performance.

Furthermore, the model accuracy is illustrated in Fig. 6. The accuracy can be defined as the ratio of true predictions to total one made by the model. At the beginning of training, accuracy usually increases rapidly as the model begins to learn the basic patterns within the data. Analogous to the loss curve, the accuracy curve likewise attains a plateau, indicating the maximal learning capability for the given data and architecture. The training data and test data exhibit comparable accuracies of 0.942 and 0.948, respectively.

The combination of increase in accuracy and reduction of loss over time indicates the effectiveness of the DNN training process. The analogous pattern of loss and accuracy for both training and unseen data

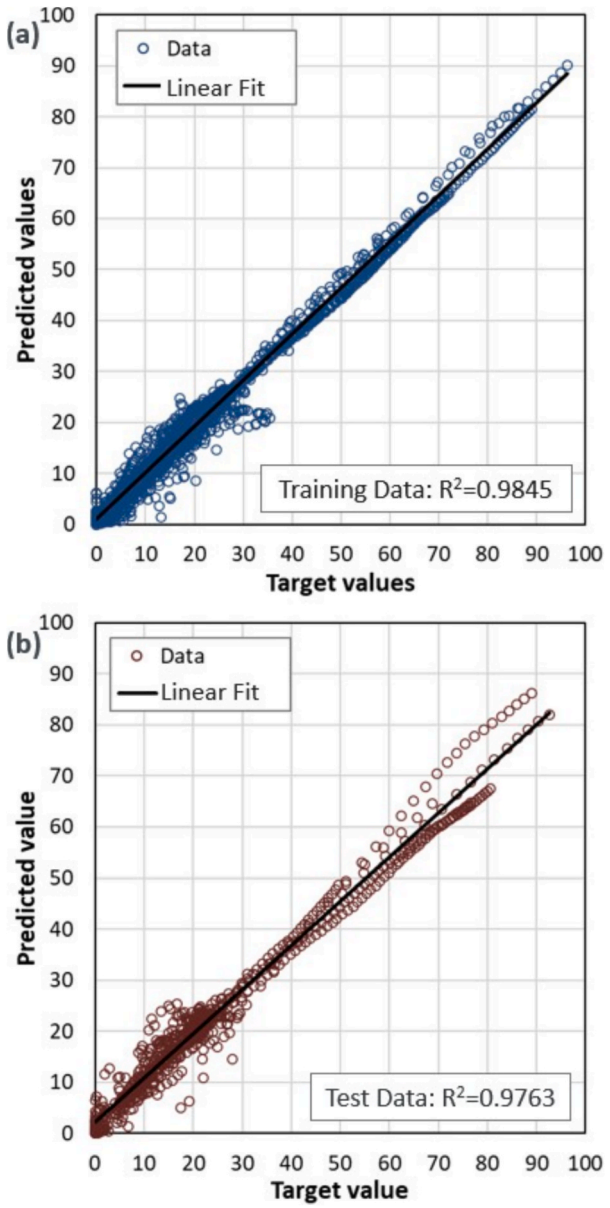

Fig. 7. Linear regression of the DNN. (a) Training values (b) Test values.

confirms the model's efficacy, demonstrating its ability to mitigate possible concerns, such as overfitting, a common problem for limited data sets. For instance, overfitting is typically marked by a persistent rise in training accuracy coupled with a plateau or rise in test loss [66]. Furthermore, both metric results corroborate the appropriate selection of hyperparameters, including the number of hidden neurons and learning rate, therefore confirming the correctness and reliability of model predictions.

In addition a linear regression between predicted and target values is depicted in Fig. 7, quantifying how much of the variance in target variables is captured by the predictions. The regression plots demonstrate a good correlation between the output values and targets, with a coefficient of determination R^2 of 0.9845 for the training data and 0.9745 for the test data. The training predictions, shown by markers, essentially coincide with a diagonal line, exhibiting minor discrepancies during the initial phase of spray development (Fig. 7a). The test predictions replicate the same behavior, with the inclusion of some over predictions that account for the long STP and initial phase of the spray, as illustrated in Fig. 7b. The early stages of spray measurement are characterized by significant flow disturbances and statistical uncertainty, resulting from the embedded complexities of spray formation, turbulence, and measuring difficulties. These factors influence the variability observed in spray characteristics and the quality of the model prediction.

Overall, these disparities can be considered minor across the entire dataset concerning the model's accuracy and reliability. Despite minor differences, the DNN consistently estimated the actual values, exhibiting a balance between fitting and predictive capabilities while avoiding overfitting.

7.2. Spray tip penetration and cone angle prediction

Fig. 8, Fig. 9, and Fig. 10 illustrate the comparison between the observed STP and SCA and their corresponding predicted values generated by the DNN. The graphs exhibit STP and SCA as a function of time after energization, showcasing the versatility of the DNN to forecast the temporal evolution of the spray in three ranges: short, medium, and long penetration length. These range classification was imposed by the authors due to the easy assimilation with the results. Besides, they also represent respectively to a pilot injection for DFICE mode, part-load for Diesel-only mode and high-load for Diesel-only model. It is important to accentuate that pilot injection for DFICE mode is not only limited to a short penetration length. It is a combination of injection pressure, ambient pressure and is mostly driven by the short injection duration, often resulting in a short penetration length.

Experimental values are represented by markers and respectively error bars, whereas the neural network forecasts are shown by a solid line. The error bars were calculated via the standard deviation of the experimental values. The DNN precisely captures the STP during short penetration, as illustrated in Fig. 8a. Nevertheless, the model slightly overestimates the initial phase of the SCA (Fig. 8b) and the fluctuation of the spray angle over time. This initial overestimation is a result of averaging 5 to 10 measurements at early injection stages, where low energization duration for the pilot injection in DFICE led to high variation in the injector opening time. After this initial phase, the model persistently exhibiting an acceptable precision, however it still insensitive to the oscillation of the SCA over time for operations conditions in the range of DFICE mode. The discrepancies pertain to the accuracy range, while the DNN effectively estimates the overall trend.

A representative case of medium length or part-load for Diesel-only mode is depicted in Fig. 9a. The spray length is accurately predicted, aligning with the experimental measurements. Furthermore, a considerable enhancement of the SCA estimation is evident in Fig. 9b. With an early stabilization of the cone angle, the DNN predicts more accurately this region. However, it still overlooks the dynamics of the cone angle, presenting only the overall trend. The last comparison illustrates a scenario of long spray length or high-load for Diesel-only mode, as shown in Fig. 10. A consistent correlation between the experimental data and predictions for STP is demonstrated in Fig. 10a. A marginal underestimation of SCA is noted across the majority of the time as shown in Fig. 10b. Nonetheless, the general tendency is well addressed by the predictions, respecting the measurement standard deviation.

Overall, the DNN successfully captures the temporal evolution of the spray, precisely reflecting the penetration dynamics during the observed time for the unseen data. An over-prediction of the SCA is noted during the initial phases of spray generation, especially in short spray lengths. This mismatch indicates that the DNN might be overestimating the initial momentum or underestimating the effects on factors like air resistance and droplet interactions during the early expansion phase, in complement to the increased statistical uncertainty to the early stages of spray measurement. Moreover, the DNN seems to only cover the average behavior of the SCA. Notwithstanding these deviations, the DNN remains an valuable tool for comprehending and predicting SCA, presenting an attractive strategy to support the optimization of spray systems independent of the operation mode.

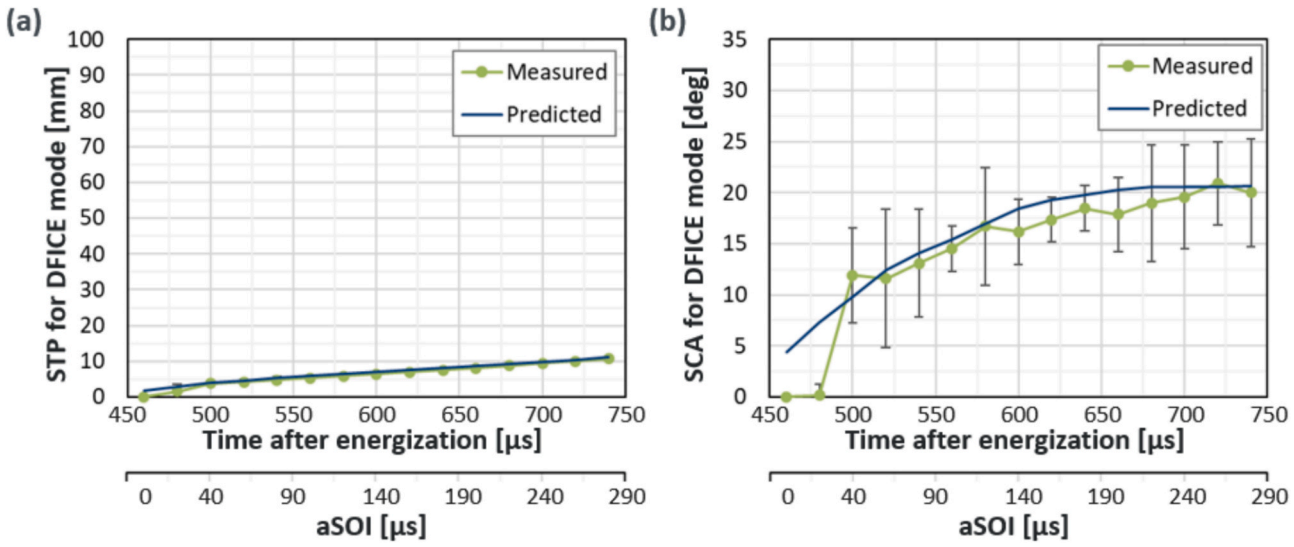

Fig. 8. Comparison of the measured and predicted STP and SCA in function of time after energization for short penetration length, a representative test case of Diesel pilot injection for DFICE mode. The injector A was tested under an injection pressure of 800 bar, ambient pressure of 50 bar and electrical pulse duration of 360 µs.

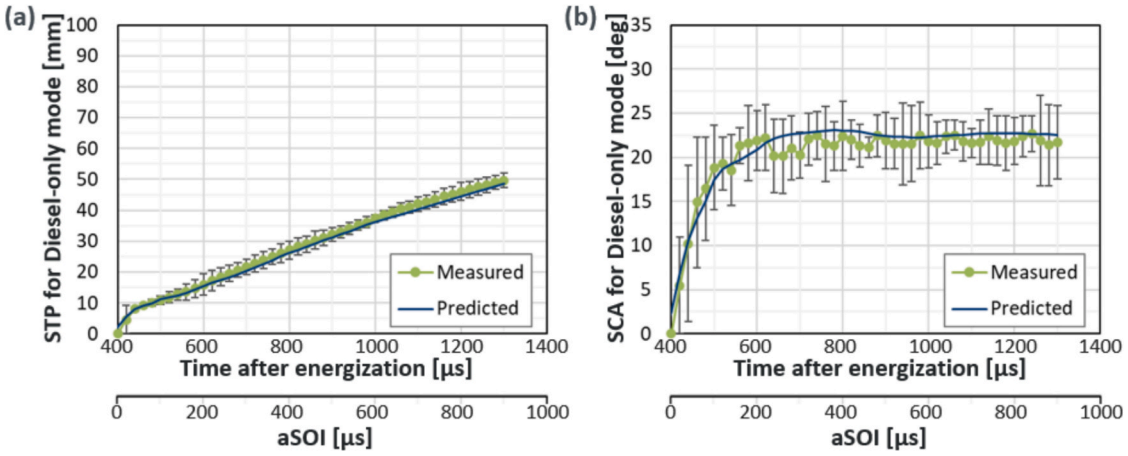

Fig. 9. Comparison of the measured and predicted STP and SCA in function of time after energization for medium penetration length, a representative test case of part-load for Diesel-only mode. The injector B was tested under an injection pressure of 1000 bar, ambient pressure of 60 bar and electrical pulse duration of 500 µs.

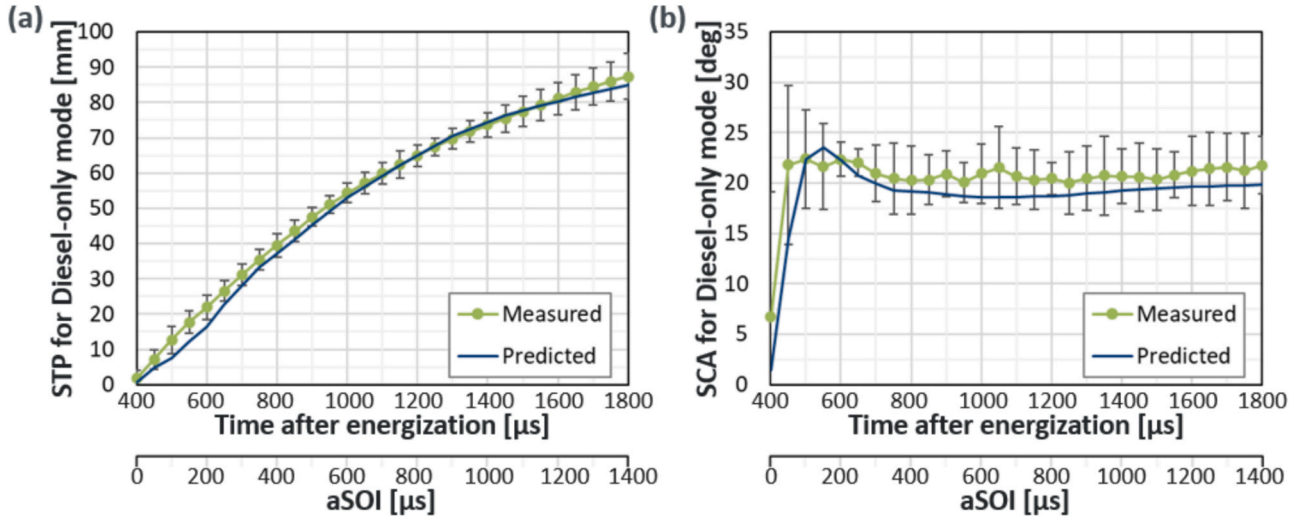

Fig. 10. Comparison of the measured and predicted STP and SCA in function of time after energization for long penetration length, a representative test case of high-load for Diesel-only model. The injector C was tested under an injection pressure of 2000 bar, ambient pressure of 47 bar and electrical pulse duration of 947 µs.

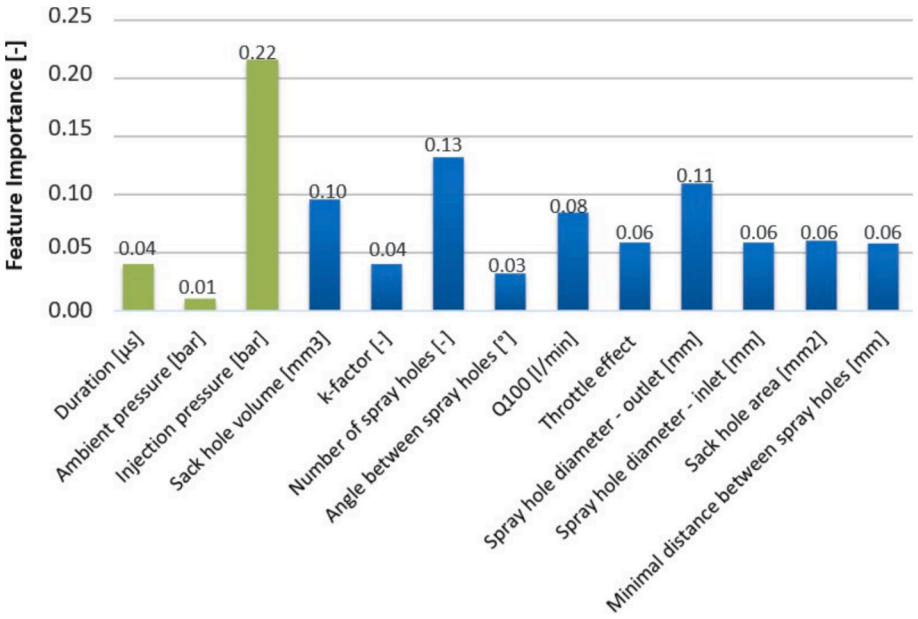

Fig. 11. Feature importance analysis of the DNN input: green bars represent the operation conditions, while blue bars geometrical parameters. (For interpretation of the references to colour in this figure legend, the reader is referred to the web version of this article.)

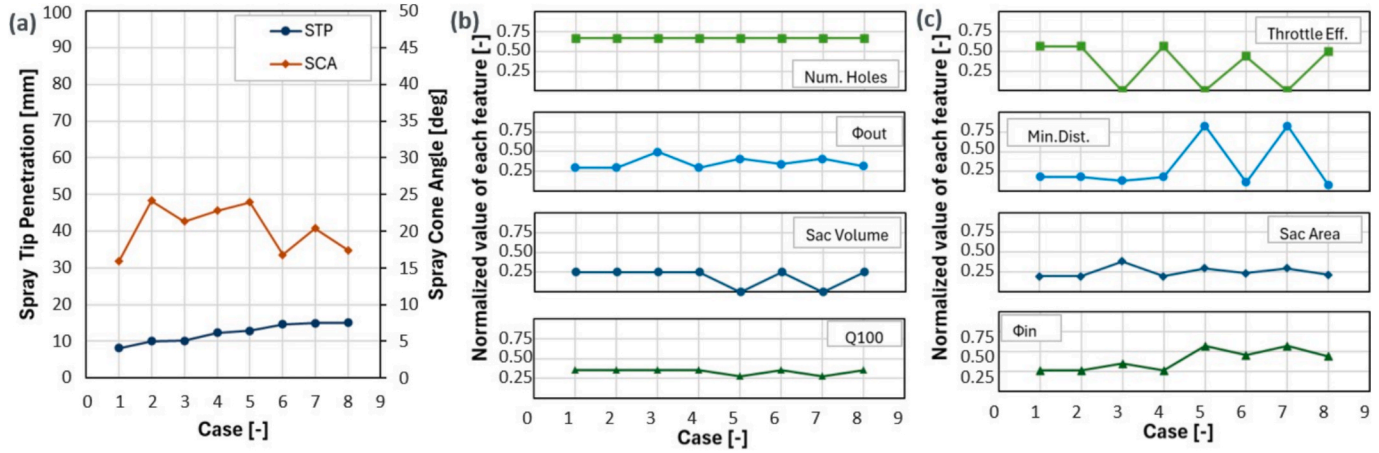

Fig. 12. Eight selected cases at operation conditions representative of pilot injection in DFICE mode: (a) Spray characteristics per selected case; (b) normalized geometrical feature with higher importance; (c) normalized geometrical feature with 0.06 importance.

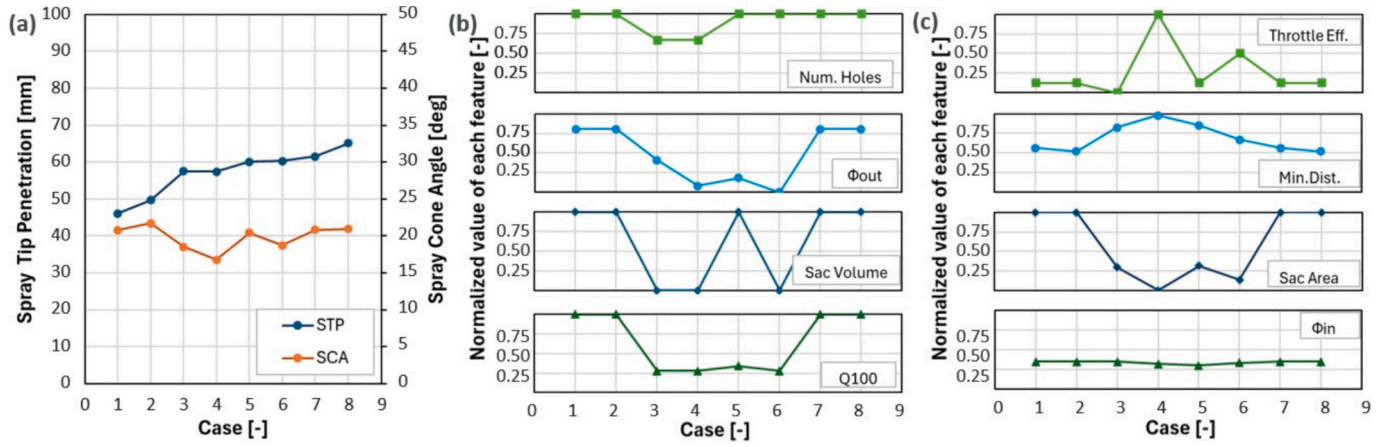

Fig. 13. Eight selected cases at operation conditions representative of part-load for Diesel-only mode. (a) Spray characteristics per selected case; (b) normalized geometrical feature with higher importance; (c) normalized geometrical feature with 0.06 importance.

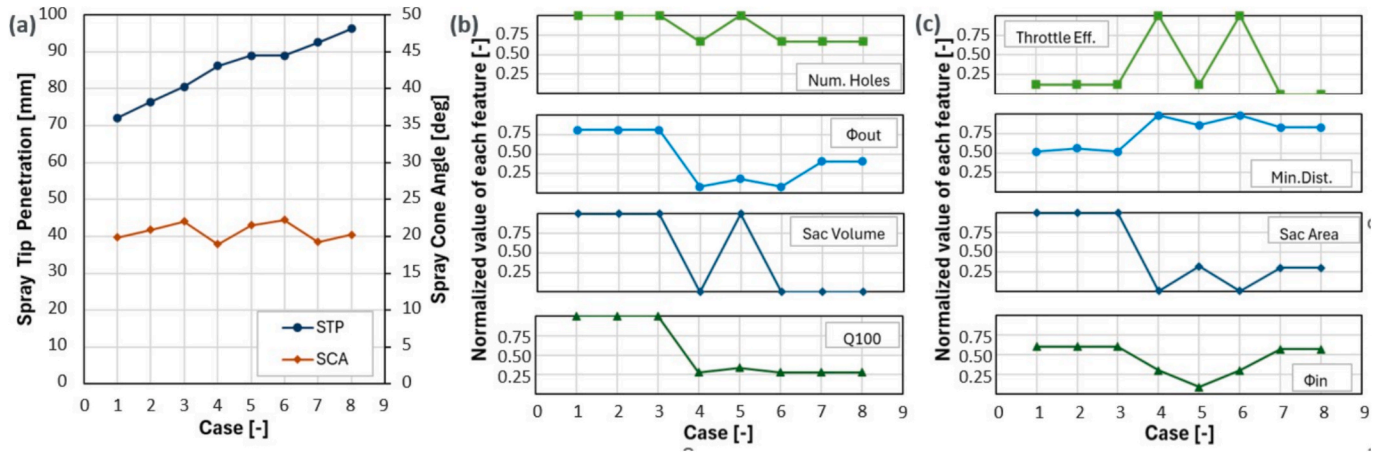

Fig. 14. Eight selected cases at operation conditions representative of high-load for Diesel-only mode: (a) Spray characteristics per selected case; (b) normalized geometrical feature with higher importance; (c) normalized geometrical feature with 0.06 importance.

Table 3
Accuracy of the training data in terms of number of hidden layer and neurons per layer.

Number of hidden layer	14 neurons per layer	28 neurons per layer	42 neurons per layer	56 neurons per layer	70 neurons per layer
5	0.936	0.944	0.950	0.942	0.950
10	0.939	0.943	0.947	0.940	0.948
14	0.933	0.939	0.937	0.933	0.942
15	**0.931**	**0.938**	**0.941**	**0.930**	**0.940**
16	0.931	0.937	0.937	0.944	0.945
17	0.933	0.941	0.946	0.936	0.944
18	0.921	0.937	0.937	0.939	0.943
19	0.931	0.938	0.939	0.933	0.939
20	0.921	0.937	0.934	0.935	0.935
25	0.931	0.932	0.928	0.931	0.927
30	0.648	0.932	0.926	0.922	0.610

Table 4
Accuracy of the test data in terms of number of hidden layer and neurons per layer.

Number of hidden layer	14 neurons per layer	28 neurons per layer	42 neurons per layer	56 neurons per layer	70 neurons per layer
5	0.909	0.914	0.943	0.948	0.945
10	0.880	0.916	0.941	0.914	0.939
14	0.907	0.918	0.950	0.934	0.950
15	**0.920**	**0.939**	**0.930**	**0.943**	**0.952**
16	0.880	0.930	0.934	0.939	0.945
17	0.932	0.930	0.909	0.927	0.945
18	0.911	0.932	0.932	0.930	0.945
19	0.934	0.948	0.932	0.930	0.934
20	0.905	0.916	0.943	0.941	0.930
25	0.918	0.934	0.932	0.932	0.923
30	0.459	0.930	0.930	0.927	0.498

7.3. Analysis of the input features influence on the DNN and spray macroscopic characteristics

Fig. 11 presents the feature importance analysis performed on the trained neural network, providing insights into the relative influence of the input features on the predicted values based on the experimental data set of this work. The graph depicts the normalized importance of each feature, ranked from most to least significant. The injection pressure is a predominant factor among the operational conditions, with an importance of 0.22. As expected, the injection pressure affects the spray momentum and topology, including spray angle [67]. Elevated pressures can result in more transient sprays characterized by greater variability in spray morphology [68]. The injection duration has an intermediate importance of 0.04, since longer injection durations often result in enhanced STP lengths and a broader dispersion pattern.

What is most striking is that the ambient pressure exhibits the least significance compared to other input features, an opposite trend that is normally found in the literature. However, this relative low importance reflects the design space of the selected experiments and more specifically to the range of this input variable in this study. The experimental measurements were carried out over the last 10 years with similar CVC back pressures. As a consequence, the ambient pressure has low variability in the input set and therefore misleads the DNN to think it has a low relative importance. This analysis only displays the relative importance of each feature, therefore partially reflecting the complete physics behind the spray development.

Since the inclusion of geometrical parameters was one of the distinctiveness of this network, those features present a more balanced relative importance and high variability in the input set. Among the geometrical parameters, the number of spray holes, spray hole outlet diameter and sac hole volume are the predominant geometrical feature affecting the learning behavior of the DNN, with respective importance of 0.13, 0.11, and 0.10. The spray hole outlet diameter is the primary geometrical parameters in most semi-empirical and ML model for spray characteristics due to their direct influence on momentum and initial droplet size [20].

Interestingly, Q100 demonstrates a relative relevance of 0.08, while the throttle effect, inlet spray hole diameter, sac hole area, and minimal distance between spray holes show equivalent importance of 0.06, indicating a complex interplay among these features. The K-factor and the angle between spray holes exhibit somewhat diminished significance, suggesting a relative reduce impact within the examined data set range.

This hierarchical interpretation of feature importance underlines which inputs features most influence the DNN. This analysis assists on the interpretability and reliability of the ML model, often referred to as "black-box" because of their complex structure [69]. Besides, their interpretation is also a reflection of the training data set and their intricate interaction on the prediction. It can show the relative significance of a input parameter, an information valuable for the injector design optimization process. However, the feature importance analysis cannot always be translated into mechanisms that governing the spray behavior. Due to this limitation in terms of physical knowledge, Physics-informed machine learning have been a growing subarea of ML, where physical laws are incorporated as model constrains or loss terms [70]. Despite their advantages, the evaluation of high-order derivatives leads to performance loss and robustness issues rendering them, up to the

present time, unfit for most real-world problems at engineering scales [71].

In complement to understanding better the correlations between the variability of the geometrical design parameters and spray characteristics for fuel flexibility, eight training set cases from each range (short, medium and long penetration length) were selected, covering the main attributes of pilot injection in DFICE mode, part-load and high-load for Diesel-only mode. This qualitative comparison gives a perception of the geometrical parameters interactions, and a perspective to narrow the design range.

Fig. 12, Fig. 13 and Fig. 14 illustrate the nominal STP and SCA of each category alongside the normalized geometrical parameters of the more relevant geometrical input feature. The geometrical parameters are normalized to facilitate direct comparison and preserve Woodward L'Orange proprietary information

Fig. 12 shows the representative cases of a short spray length. The STP below 20 mm was artificially imposed to select those cases, where the SCA fluctuates between 15 and 25 degrees, as displayed in Fig. 12a. The normalized geometrical parameters that have higher to medium importance (greater than 0.07) are presented in Fig. 12b, while those of medium importance (0.06) are depicted in Fig. 12c. The number of spray holes, outlet spray hole diameter, sac hole volume, Q100, inlet spray hole diameter and sac hole area showed minimal variation. The throttle effect presented considerable variation, while the minimal distance between spray holes revealed more variability for penetrations over 12 mm. Consequently, when designing injectors for short penetration, most geometrical parameters may be specified within a more narrow range, disregarding the operational conditions.

The medium spray length examples are depicted in Fig. 13, where the STP ranging from 45 to 65 mm was the selected cut, with a corresponding SCA around 20 degrees. The number of spray holes, inlet spray hole diameter and minimal distance between spray holes are the sole characteristics with limited variability. When designing injector targeting this spray characteristics range, those variable present limited design space, showing pronounced design tendency. The other geometrical parameters, owing to considerable variability and unclear trends, may provide for broader conceptual flexibility when addressing this performance range.

Finally, the long penetration length is illustrated in Fig. 14. For penetration ranges above 70 and 80 mm, all geometrical parameters remain at generally steady levels, indicating a strong design tendency. As penetration exceeds 80 mm, the number of spray holes, inlet spray hole diameter, Q100, minimal distance between spray holes and sac area oscillate within a limited range after an abrupt shift in tendency, underlining the need for careful consideration in their design space. Nevertheless, the sac hole volume, throttle effect, and inlet spray hole diameter may provide more conceptual versatility.

8. Conclusions

In this work, a DNN was implemented to predict the macroscopic characteristics of marine diesel injectors, focusing on the fuel flexibility during engine operation in both DFICE and Diesel-only modes. The model was designed to support the early injector design phase, incorporating a larger number of geometrical characteristics, with 10 design features integrated into the DNN formulation. In addition, the experimental measurements of 27 injector designs under various operational conditions were utilized to train the DNN, which resulted in a total of 85 experimental test cases. The combination of the 3 operating condition as input features (injection pressure, ambient pressure and injection duration) cover the range of conditions relevant to fuel flexibility: pilot injection in DFICE mode, part-load and high-load for Diesel-only mode.

The large numbers of inputs features based on different injector designs bring distinctiveness to this neural network. In the same time, this distinguish characteristic in combination with limited experimental data set size have considerably increased the model complexity. The proposed DNN architecture and fine-tuning of the hyperparameters associated to the regularization techniques have ensured a responsive performance, mitigation of overfit issues and effective generalization. The neural network exhibits strong predictive capabilities for STP and SCA independent of the operation mode, with an accuracy of 95 % for the unseen data.

The feature importance analysis performed on the trained neural network offers an additional perspective of the main influences on the DNN for the predictions. This relative comparison do not directly translate into mechanisms that governing the spray behavior. However, it underlines the learning behavior of the neural network and the characteristics of the training data set. In this perspective, the injection pressure (operation condition) holds the highest importance among all features. For the geometrical parameters, the number of spray holes and spray hole outlet diameter exhibit the most influence on the DNN. Additionally, certain geometrical parameters can potentially be categorized within a restricted or extensive range concerning design space and injector target performance. Finally, the proposed DNN can support the marine injector design process due to the fast exploration of the design range in respect of geometrical constrains and identification of promising designs in the early phase more effectively in terms of STP and SCA. This gain in time would contribute to accelerate the optimization process, allowing to focus on fine-tune and validate the design in the next stages of the development phase.

CRediT authorship contribution statement

Marilia G.J. Vaz: Writing – review & editing. **Ioannis Karathanassis:** Writing – review & editing, Supervision, Project administration, Funding acquisition. **Manolis Gavaises:** Writing – review & editing, Supervision, Project administration, Funding acquisition. **Gerard Mouokue:** Writing – review & editing.

Declaration of competing interest

The authors declare that they have no known competing financial interests or personal relationships that could have appeared to influence the work reported in this paper.

Acknowledgments

This work has received funding from the European Union's Horizon 2020 research and innovation program under the Marie Sklodowska-Curie grant agreement No 861002.

Appendix A. . DNN architecture — number of hidden layers

The number of hidden layers was determined via sensibility study. Since the time for training the network was similar independent of their complexity due to the limited size of the data set. The accuracy was the chosen criteria for the optimal number of layers. Table 3 and Table 4 summarizes the accuracy of the training and test data related to the combination of number of hidden layer and neurons per layer, where all other hyperparameters were kept constant. 15 hidden layers presented a good best trade-off between training and test accurate.

Data availability

The data that has been used is confidential.

References

[1] Kirolivanos G, Jeong B. Comparative reliability analysis and enhancement of marine dual-fuel engines. J Int Maritime Saf, Environ Affair Shipp 2022;6:1–23.
[2] Mohd Noor C, Noor M, Mamat R. Biodiesel as alternative fuel for marine diesel engine applications: a review. Renew Sustain Energy Rev 2018;94:127–42.

[3] Roskilly A, Palacin R, Yan J. Novel technologies and strategies for clean transport systems. Appl Energy 2015;157:563–6.
[4] Sharples J. Lng supply chains and the development of lng as a shipping fuel in northern Europe. The Oxford Institute for Energy Studies 2019.
[5] Ni P, Wang X, Li H. A review on regulations, current status, effects and reduction strategies of emissions for marine diesel engines. Fuel 2020;279:118477.
[6] Deng J, Wang X, Wei Z, Wang L, Wang C, Chen Z. A review of nox and sox emission reduction technologies for marine diesel engines and the potential evaluation of liquefied natural gas fuelled vessels. Sci Total Environ 2021;766:144319.
[7] M. D. Kass, Z. Abdullah, M. J. Biddy, C. Drennan, Z. Haq, T. Hawkins, S. Jones, J. Holliday, D. E. Longman, S. Menter, E. Newes, T. J. Theiss, T. Thompson, M. Wang, Understanding the opportunities of biofuels for marine shipping, Department of Energy's (DOE) (2018).
[8] Foretich A, Zaimes GG, Hawkins TR, Newes E. Challenges and opportunities for alternative fuels in the maritime sector. Marit Transport Res 2021;2:100033.
[9] J. Klimstra, 11 - fuel flexibility with dual-fuel engines, in: J. Oakey (Ed.), Fuel Flexible Energy Generation, Woodhead Publishing, Boston, 2016, pp. 293–304. URL: https://www.sciencedirect.com/science/article/pii/B9781782423782000110. doi: 10.1016/B978-1-78242-378-2.00011-0.
[10] Sahoo B, Sahoo N, Saha U. Effect of engine parameters and type of gaseous fuel on the performance of dual-fuel gas diesel engines—a critical review. Renew Sustain Energy Rev 2009;13:1151–84.
[11] Watanabe K. High operation capable marine dual fuel engine with lng. Mar Eng 2015;50:738–43.
[12] Kim K, Kim D, Jung Y, Bae C. Spray and combustion characteristics of gasoline and diesel in a direct injection compression ignition engine. Fuel 2013;109:616–26.
[13] Nishida K, Zhu J, Leng X, xia He Z. Effects of micro-hole nozzle and ultra-high injection pressure on air entrainment, liquid penetration, flame lift-off and soot formation of diesel spray flame. Int J Engine Res 2017;18:51–65.
[14] Wakuri Y, Fujii M, Amitani T, Tsuneya R. Studies on the penetration of fuel spray in a diesel engine. Bull JSME 1960;3:123–30.
[15] Hiroyasu H, Arai M. Structures of fuel sprays in diesel engines. Soc Automot Eng 1990.
[16] Zhou X, Li T. Modeling of the entire processes of diesel spray tip penetration including the start- and end-of-injection transients. J Energy Inst 2021;98:271–81.
[17] Kaario OT, Karimkashi S, Bhattacharya A, Vuorinen V, Larmi M, Bai X-S. A comparative study on methanol and n-dodecane spray flames using large-eddy simulation. Combust Flame 2024;260:113277.
[18] Afzal A, Ansari Z, Faizabadi AR, Ramis M. Parallelization strategies for computational fluid dynamics software: State of the art review. Arch Comput Meth Eng 2016;24:337–63.
[19] Paredi D, Lucchini T, D'Errico G, Onorati A, Pickett L, Lacey J. Validation of a comprehensive computational fluid dynamics methodology to predict the direct injection process of gasoline sprays using spray g experimental data. Int J Engine Res 2020;21:199–216.
[20] Liu L, Peng Y, Liu D, Han C, Zhao N, Ma X. A review of phenomenological spray penetration modeling for diesel engines with advanced injection strategy. Int J Spray Combust Dynam 2020;12:1756827720934067.
[21] Nowruzi H, Ghassemi H, Amini E, Sohrabi-asl I. Prediction of impinging spray penetration and cone angle under different injection and ambient conditions by means of cfd and anns. J Braz Soc Mech Sci Eng 2017;39:3863–80.
[22] Hwang J, Lee P, Mun S, Karathanassis I, Koukouvinis P, Pickett L, et al. Machine-learning enabled prediction of 3d spray under engine combustion network spray g conditions. Fuel 2021.
[23] Liu Y, Tian J, Song Z, Li F, Zhou W, Lin Q. Spray characteristics of diesel, biodiesel, polyoxymethylene dimethyl ethers blends and prediction of spray tip penetration using artificial neural network. Phys Fluids 2022;34:015117.
[24] Richards B, Emekwuru N. Prediction of spray vapor tip penetration of diesel, biodiesel and synthetic fuels using artificial neural networks with confidence intervals. SAE Technical Paper 2023.
[25] Khan S, Masood M, Medina M, Alzahrani F. Advancing fuel spray characterization: a machine learning approach for directly injected gasoline fuel sprays. Fuel 2024;371:131980.
[26] Zhang Y, Zhang G, Wu D, Wang Q, Nadimi E, Shi P, et al. Parameter sensitivity analysis for diesel spray penetration prediction based on ga-bp neural network. Energy AI 2024;18:100443.
[27] Tian J, Liu Y, Bi H, Li F, Bao L, Han K, et al. Experimental study on the spray characteristics of octanol diesel and prediction of spray tip penetration by ann model. Energy 2022;239:121920.
[28] Zhang Y, Su Y, Li X, Xie F, Yu H, Shen B, et al. Study and prediction on macroscopic characteristics of free spray of typical alcohol fuels through experimentation and the artificial neural network. Energy 2025;316:134610.
[29] Zhang Y, Su Y, Li X, Xie F, Wang Y, Shen B, et al. Modeling of spray characteristics of alcohol fuels using response surface methodology and artificial neural networks. Fuel 2025;392:134936.
[30] Leng X, Xing M, Luo Z, Jin Y, He Z, Wei S. An investigation on methanol high pressure spray characteristics and their predictive models. Energy 2024;313:133732.
[31] B. Dherin, M. Munn, M. Rosca, D. G. Barrett, Why neural networks find simple solutions: the many regularizers of geometric complexity, in: Proceedings of the 36th International Conference on Neural Information Processing Systems, NIPS '22, Curran Associates Inc., Red Hook, NY, USA, 2022.
[32] Kavzoglu T, Mather P. The role of feature selection in artifial neural network applications. Int J Remot Sens 2002;23:2919–37.
[33] Jeyaseelan T, Son M, Sander T, Zigan L. Experimental and modeling analysis of the transient spray characteristics of cyclopentane at sub- and transcritical conditions using a machine learning approach. Phys Fluids 2023;35.
[34] S. E. Whang, Y. Roh, H. Song, J. Lee, Data collection and quality challenges in deep learning: A data-centric AI perspective, CoRR abs/2112.06409 (2021).
[35] Shi Q, Hu Y, Yan G. Fault diagnosis of me marine diesel engine fuel injector with novel ircmde method. Pol Marit Res 2023;30:96–110.
[36] Dent J. A basis for the comparison of various experimental methods for studying spray penetration. Soc Automot Eng 1971.
[37] Naber JD, Siebers DL. Effects of gas density and vaporization on penetration and dispersion of diesel sprays. SAE Trans 1996;105:82–111.
[38] Desantes J, Payri R, Salvador F, Gil A. Development and validation of a theoretical model for diesel spray penetration. Fuel 2006;85:910–7.
[39] K. Najar, C. Fink, F. Pinkert, H. Harndorf, A new spray penetration model developed for large engine diesel injectors, ILASS – Europe 2014, 26th Annual Conference on Liquid Atomization and Spray Systems (2014).
[40] Zhang W, Li X, Huang L, Feng M. Experimental study on spray and evaporation characteristics of diesel-fueled marine engine conditions based on optical diagnostic technology. Fuel 2019;246:454–65.
[41] Varde KS, Popa DM, Varde LK. Spray angle and atomization in diesel sprays. SAE Trans 1984;93:779–87.
[42] Arrègle J, Pastor JV, Ruiz S. The influence of injection parameters on diesel spray characteristics. SAE Technical Paper 1999.
[43] Payri R, Salvador F, Bracho G, Viera A. Vapor phase penetration measurements with both single and double-pass schlieren for the same injection event. In: in: 28th Conference on Liquid Atomization and Spray Systems; 2017. https://doi.org/10.4995/ILASS2017.2017.4884.
[44] Bottega A, Dongiovanni C. Diesel spray macroscopic parameter estimation using a synthetic shapes database. Appl Sci 2019;9.
[45] A. R. Lowe, B. Jasiok, V. V. Melent'ev, O. S. Ryshkova, V. I. Korotkovskii, A. K. Radchenko, E. B. Postnikov, M. Spinnler, U. Ashurova, J. Safarov, E. Hassel, M. Chorążewski, High-temperature and high-pressure thermophysical property measurements and thermodynamic modelling of an international oil standard: Ravenol diesel rail injector calibration fluid, Fuel Processing Technology 199 (2020) 106220.
[46] Safarov J, Ashurova U, Ahmadov B, Abdullayev E, Shahverdiyev A, Hassel E. Thermophysical properties of diesel fuel over a wide range of temperatures and pressures. Fuel 2018;216:870–89.
[47] Amin A, Gadallah A, El Morsi A, El-Ibiari N, El-Diwani G. Experimental and empirical study of diesel and castor biodiesel blending effect, on kinematic viscosity, density and calorific value. Egypt J Pet 2016;25:509–14.
[48] Zhang T, Zhu T, Xiong P, Huo H, Tari Z, Zhou W. Correlated differential privacy: Feature selection in machine learning. IEEE Trans Ind Inf 2020;16:2115–24.
[49] Puth M-T, Neuhäuser M, Ruxton GD. Effective use of spearman's and kendall's correlation coefficients for association between two measured traits. Anim Behav 2015;102:77–84.
[50] Farlie DJG. The performance of some correlation coefficients for a general bivariate distribution. Biometrika 1960;47:307–23.
[51] Arndt S, Turvey C, Andreasen NC. Correlating and predicting psychiatric symptom ratings: Spearmans r versus kendalls tau correlation. J Psychiatr Res 1999;33:97–104.
[52] Mishra S, Pradhan R. Analyzing the impact of feature correlation on classification acuracy of machine learning model. In: 2023 International Conference on Artificial Intelligence and Smart Communication (AISC); 2023. p. 949–53.
[53] Jiang L, Zhang L, Li C, Wu J. A correlation-based feature weighting filter for naive bayes. IEEE Trans Knowl Data Eng 2019;31:201–13.
[54] Schratz P, Muenchow J, Iturritxa E, Cortés J, Bischl B, Brenning A. Monitoring forest health using hyperspectral imagery: does feature selection improve the performance of machine-learning techniques? Remote Sens 2020;13:4832.
[55] Kaneko H. Interpretation of machine learning models for data sets with many features using feature importance. ACS Omega 2023;8:23218–25.
[56] Janiesch C, Zschech P, Heinrich K. Machine learning and deep learning. Electron Mark 2021;31:685–95.
[57] Schmidhuber J. Deep learning in neural networks: an overview. Neural Netw 2015;61:85–117.
[58] Adil M, Ullah R, Noor S, Gohar N. Effect of number of neurons and layers in an artificial neural network for generalized concrete mix design. Neural Comput Applic 2020;34:8355–63.
[59] Wan W, Mabu S, Shimada K, Hirasawa K, Hu J. Enhancing the generalization ability of neural networks through controlling the hidden layers. Appl Soft Comput 2009;9:404–14.
[60] Maniatopoulos A, Mitianoudis N. Learnable leaky relu (lelelu): an alternative accuracy-optimized activation function. Information 2021;12.
[61] N. Srivastava, G. E. Hinton, A. Krizhevsky, I. Sutskever, R. Salakhutdinov, Dropout: a simple way to prevent neural networks from overfitting, J. Mach. Learn. Res. 15 (2014) 1929–1958.
[62] Zunino A, Bargal SA, Morerio P, Zhang J, Sclaroff S, Murino V. Excitation dropout: encouraging plasticity in deep neural networks. Int J Comput Vis 2018;129:1139–52.
[63] Vardasbi A, de Rijke M, Dehghani M. Intersection of parallels as an early stopping criterion. Proceedings of the 31st ACM International Conference on Information and Knowledge Management. 2022.
[64] Wu X, Xiang B, Lu H, Li C, Huang X, Huang W. Optimizing recurrent neural networks: a study on gradient normalization of weights for enhanced training efficiency. Appl Sci 2024.

[65] Zhang T, Zhu T, Gao K, Zhou W, Yu PS. Balancing learning model privacy, fairness, and accuracy with early stopping criteria. IEEE Trans Neural Networks Learn Syst 2021;34:5557–69.
[66] Abad-Rocamora E, Liu F, Chrysos GG, Olmos P, Cevher V. Efficient local linearity regularization to overcome catastrophic overfitting. ArXiv abs/240111618 2024.
[67] Shi Z, Lee C, Wu H, Li H, Wu Y, Zhang L, et al. Effect of injection pressure on the impinging spray and ignition characteristics of the heavy-duty diesel engine under low-temperature conditions. Appl Energy 2020;262:114552.
[68] Salvador FJ, Gimeno J, Morena J, González-Montero LA. Experimental analysis of the injection pressure effect on the near-field structure of liquid fuel sprays. Fuel 2021;292:120296.
[69] Grisci BI, Krause MJ, Dorn M. Relevance aggregation for neural networks interpretability and knowledge discovery on tabular data. Inf Sci 2021;559:111–29.
[70] Xu C, Cao BT, Yuan Y, Meschke G. Transfer learning based physics-informed neural networks for solving inverse problems in engineering structures under different loading scenarios. Comput Methods Appl Mech Eng 2023;405:115852.
[71] Sinha U, Dindoruk B. Review of physics-informed machine learning (piml) methods applications in subsurface engineering. Geoenergy Sci Eng 2025;250:213713.